communications materials

Article

https://doi.org/10.1038/s43246-024-00467-7

Taming *cyclo*-pentazolate anions with a hydrogen-bonded organic framework

Yuangang Xu[1,2] ✉, Jianxin Zhou[1,2], Xinyi Li[1], Tianyang Hou[1], Ze Xu[1], Pengcheng Wang[1] & Ming Lu[1] ✉

Because of its high energy, aromaticity, and carbon- and hydrogen-free structure, the *cyclo*-pentazolate anion (*c*-N_5^-) has attracted increased attention as a potential polynitrogen structural unit for the research of next-generation high energy density materials. However, the poor thermal stability of *c*-N_5^--based compounds has become an important factor restricting their development. Here, we show that a hydrogen-bonded organic framework (HOF) self-assembles with and stabilizes *c*-N_5^-, with *c*-N_5^- situated in the pores of the resulting framework through the formation of symmetrical *c*-N_5^- hydrogen bonds as the main stabilizing factors. These factors result in an onset decomposition temperature of 153 °C for the *c*-N_5^-@HOF portion, which exceeds the thermal stabilities generally observed for *c*-N_5^--based derivatives of below 135 °C. We envisage that further *c*-N_5^--based materials with enhanced stabilities and better performance will be developed in the future.

High energy density materials (HEDMs) have seen extensive use in explosives, propellants, and pyrotechnics, and the defense industry has realized rapid development[1]. With increasing demand for HEDMs in modern weapons, traditional CHON-based energetic compounds (2,4,6-trinitrotoluene, 1,3,5-trinitro-1,3,5-triazacyclohexane, 1,3,5,7-tetranitro-1,3,5,7-tetraazacyclooctatane, and 2,4,6,8,10,12-hexanitro-2,4,6,8,10,12-hexaazaisowurzitane, etc.) are facing the bottleneck of limited theoretical energies[2].

One of the latest developments in HEDMs is high nitrogen and polynitrogen compounds[3]. The energy contents of these materials come from the high enthalpies of formation for extended single- and double-bonded nitrogen systems (N—N, N═N, N—C, N═C, N—O, etc.)[4]. Nitrogen chemistry is very different from carbon chemistry. Increasing the bond order of nitrogen leads to a higher average bond energy (BE), rather than a lower bond energy as seen for carbon ($BE_{N\equiv N} > 2 \times BE_{N=N} > 3 \times BE_{N-N}$; $BE_{C\equiv C} < 2 \times BE_{C=C} < 3 \times BE_{C-C}$; Supplementary Table 14)[5]. In practice, this implies that carbon compounds form stable polymers, whereas nitrogen compounds form stable monomers. Natural allotropic modifications of nitrogen, except for molecular nitrogen (N_2), have not been found[6]. Due to this special property, the formation of N_2 (triple bond) from single and double nitrogen bonds releases large amounts of energy[7]. This approach is attractive for use in HEDMs, but it also means that polynitrogen compounds are metastable, making their syntheses and characterization extremely challenging.

To date, only three stable polynitrogen ions, namely, N_3^-, N_5^+, and *c*-N_5^-, have been bulk synthesized at room temperature and pressure. The azide anion N_3^-[8] was first isolated by T. Curtius in 1890. After 109 years, a salt containing the N_5^+ cation was synthesized in 1999 for the first time[9]. Then, the stable, aromatic, and planar *c*-N_5^- anion was discovered in 2017, and polynitrogen chemistry expanded[10–12]. Within 5 years, *c*-N_5^- had been used in the syntheses of various energetic materials, including metallic salts, complexes, metal-pentazolate frameworks, coordination polymers, organic salts, and energetic cocrystals[13–25]. Unfortunately, the stabilities and high energy contents are contradictory, especially for catenated nitrogen systems. Almost all compounds containing *c*-N_5^- decompose at 80–130 °C[26].

For more than half a century, many attempts have been made to inrease the thermal stability of *c*-N_5^-, such as the construction of arylpentazole, three-dimensional (3D) metal-pentazolate frameworks[15,21] or cocrystals[22]. The thermal stabilities of these materials continue to increase, surpassing those of N_5^+ derivatives (22–70 °C)[9,27–29], but still have not reached 150 °C. It is important to increase the thermal stabilities before these materials can be included in advanced energetic materials. Otherwise, poor thermal stabilities may become a key limiting factor in future applications.

The esthetically pleasing 3D lithium-pentazolate framework we synthesized in 2021[21] is the most thermally stable (133 °C) of all metal-*c*-N_5^- compounds. It consists of lithium and *c*-N_5^- ions, wherein the *c*-N_5^- cyclic ligands are preternaturally stabilized in this inorganic open framework featuring two types of nanocavities ($Li_{20}(N_5)_{12}$ and $Li_{24}(N_5)_{12}$) formed with strong coordination bonds (Fig. 1a). However, biguanidinium pentazolate[19]

[1]School of Chemistry and Chemical Engineering, Nanjing University of Science and Technology, Nanjing 210094, China. [2]These authors contributed equally: Yuangang Xu, Jianxin Zhou. ✉e-mail: yuangangxu@163.com; luming@njust.edu.cn

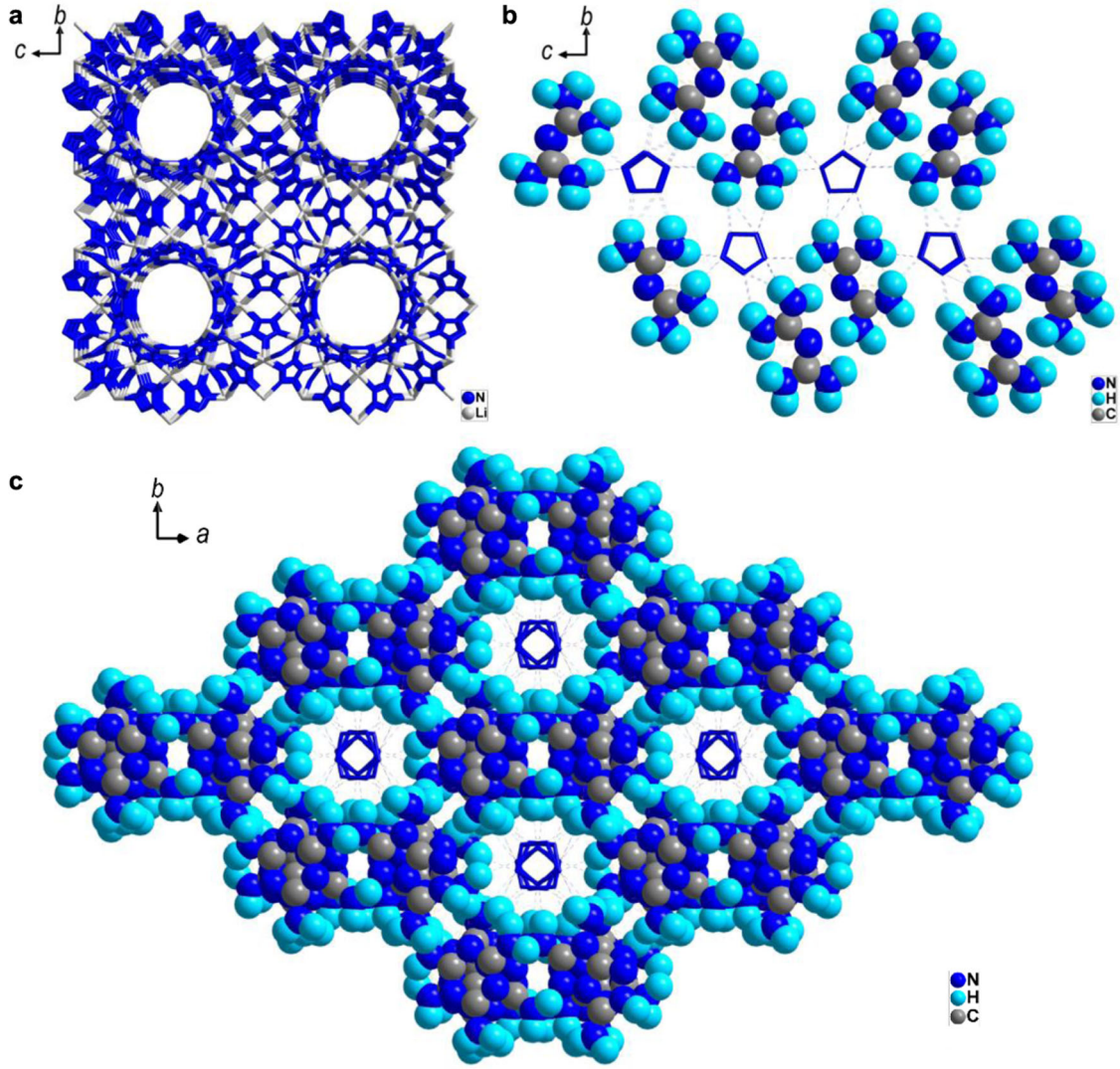

Fig. 1 | Structures of relatively thermally stable *c*-N_5^- containing compounds. a Lithium-pentazolate framework. **b** Biguanidinium pentazolate. **c** *c*-N_5^-@HOF (this work).

has the highest thermal decomposition temperature (125 °C) among all metal-free *c*-N_5^- salts (Fig. 1b). Two biguanidinium cations form dimers through paired N9—H9B…N8 (2.06 Å) hydrogen bonds, which are surrounded by 14 N—Hs and no hydrogen bond acceptor sites are exposed (Supplementary Fig. 9). However, *c*-N_5^- as a hydrogen bonding acceptor is fixed in the channel between dimers without any bonding interactions between them. The relatively high thermal stability of this compound is attributed to extensive hydrogen bonding.

As an emerging class of functional porous materials, hydrogen-bonded organic frameworks (HOFs) assembled from organic units with intermolecular hydrogen bonds have shown great potential for various applications[30–32]. In 2021, Zhang et al. designed and constructed an energetic NF@HOF (NF: nitroformate ion) by self-assembly, and the nitroformate guest ion showed a decomposition temperature of 200 °C, which was the first thermal stability above 180 °C[33]. Like the nitroformate ion, the *c*-N_5^- anion is actually a good hydrogen bond acceptor. If *c*-N_5^- guest anions occupied the pores of the designed HOF via paired hydrogen bonds and were connected by many N…H hydrogen bonds, the thermal stability of the encapsulated *c*-N_5^- would likely improve markedly.

In this work, a HOF that stabilized *c*-N_5^- was designed and constructed through self-assembly of melaminium pentazolate (MaN_5) and 3,6,7-triamine-7*H*-[1,2,4]triazole[4,3-*b*][1,2,4]triazole (TATOT), wherein *c*-N_5^- was captured in pores with diameters of 5.4 Å via formation of symmetrical *c*-N_5^- hydrogen bonds. Under the combined effects of hydrogen bonding, π–π interactions, and the framework structure, the *c*-N_5^- in *c*-N_5^-@HOF exhibited a lower electrostatic potentials (ESPs), weaker distortion, a higher Laplacian bond order, and greater aromaticity than other *c*-N_5^- derivatives. These factors resulted in *c*-N_5^-@HOF thermal stability at 153 °C (onset), surpassing those of all reported *c*-N_5^- based compounds. The detonation velocity and pressure of *c*-N_5^-@HOF were calculated as 8.029 km s^{-1} and 24.6 GPa, respectively, which were higher than those of $TATOT^+N_5^-$ (7.791 km s^{-1}, 24.6 GPa) and 2,4,6-trinitrotoluene (6.881 km s^{-1}, 19.5 GPa). In addition, *c*-N_5^-@HOF was insensitive to impact and friction. Encapsulation of *c*-N_5^- in HOFs will open the door to stable *c*-N_5^- and overcome the problems of poor thermal stability and high sensitivity.

Results

Syntheses

Silver pentazolate (AgN_5)[19], melamine hydrochloride[34] and TATOT[35] were synthesized according to previously reported procedures. MaN_5 was obtained by the metathesis of AgN_5 with melamine hydrochloride. MaN_5 and TATOT were used to assemble a new compound (*c*-N_5^-@HOF, Fig. 1c) in water at 40 °C. All of the newly synthesized compounds were characterized with nuclear magnetic resonance (NMR), infrared (IR) spectroscopy, high-resolution mass spectrometry, differential scanning calorimetry (DSC), thermogravimetric analysis (TG), and elemental analyses

(Supplementary Figs. 24–27). For detailed descriptions of the synthetic processes and the analytical data, please refer to the Methods section. *c*-N_5^-@HOF was stable in air and could be stored for extended periods (see Supplementary Note 10 and Figs 29–30). In addition, it was soluble in water and dimethyl sulfoxide, slightly soluble in methanol and ethanol, but insoluble in dichloromethane and ethyl acetate.

Single-crystal structure

The single-crystal structures of MaN_5 and *c*-N_5^-@HOF were determined with X-ray diffraction (see Supplementary Data 1–2). The crystallographic data and data collection parameters, selected bond lengths, bond angles, and hydrogen bonds are listed in Supplementary Tables 1–10.

MaN_5 crystallized with melamine and water molecules in the triclinic $P\bar{1}$ space group, and the density was 1.579 g cm^{-3} at 296 K (Supplementary Fig. 1). Each unit had four melaminium cations, four *c*-N_5^- anions, four neutral melamine molecules, and four water molecules. Along the *b*-axis, the crystal was stacked with N—H…N and O—H…N hydrogen bonds to form a framework structure with 1D pores. However, a 3D cube layer was stacked along the *c*-axis (Supplementary Fig. 2). The melaminium cations, *c*-N_5^- anions, and neutral melamine molecules were connected with many N—H…N hydrogen bonds to form wavy planes (Supplementary Fig. 2b) containing two types of rings (labeled in rose red and orange; composed of three melaminium cations, three neutral melamine molecules, and two water molecules). Water molecules served as key nodes for ring formation via a pair of N—H…O and O—H…N hydrogen bonds (orange ring: 1.8771(20) Å and 2.1796(253) Å; rose red ring: 1.9334(20) Å and 2.0963(259) Å). Melaminium cations and neutral melamine molecules are arranged alternately in each ring and were connected by paired hydrogen bonds (2.0625(20)−2.2147(21) Å) formed between the amino groups and N atoms of the triazine rings. Two types of *c*-N_5^- anions were embedded in the two types of ring centers and stabilized by five and six hydrogen bonds from species on the ring (*c*-N_5^- (N1-N5): 2.3245(30)–2.6069(22) Å (N—H…N); *c*-N_5^- (N6-N10): 2.257(2)–2.4908(20) Å (N—H…N), 1.9201(192) Å (O—H…N)), respectively (Supplementary Figs. 3, 4).

c-N_5^-@HOF crystallized in the monoclinic space group *C*2/*c* with eight molecules per unit cell ($Z = 8$) and a density of 1.688 g cm^{-3} at 100 K (CCDC 2286232). The asymmetric unit was crystallographically independent with one neutral melamine molecule, one $TATOT^+$ cation, and one *c*-N_5^- anion (Supplementary Fig. 5). As shown in Fig. 2, the neutral melamine molecules and $TATOT^+$ cations were connected through many paired N—H…N hydrogen bonds to form a plane (Fig. 2a) containing 3 + 3 membered rings (composed of three neutral melamine molecules, three $TATOT^+$ cations, and twelve hydrogen bonds) (Fig. 2b). Each ring shared all of its edges with the six surrounding rings. The lengths of the hydrogen bonds on each 3 + 3 membered ring ranged from 1.9654(19) Å to 2.2779(184) Å. It is interesting that the longest and shortest hydrogen bonds were paired between the $TATOT^+$ cation and the melamine molecule. The two pairs of hydrogen bonds between the three melamine molecules had lengths of 2.1131(205) Å and 2.1658(22) Å, respectively, and each pair of hydrogen bonds was of equal length (Supplementary Fig. 7). Along the *b*-axis, HOF showed layer-by-layer packing (Fig. 2a) with interlayer distances of ~3.2 Å. Two weak N…H9A hydrogen bonds with lengths of 2.7305(390) and 2.8400(371) Å connected adjacent layers to form a positive 3D hydrogen-bonded organic framework with pore diameters of ~5.4 Å (Fig. 2c and Supplementary Fig. 6).

The *c*-N_5^- anions were located at the centers of 3 + 3 membered rings and were coplanar with the rings (Fig. 3a–c). Each *c*-N_5^- anion was connected to seven hydrogen bonds, with bond lengths ranging from 1.9650(22) to 2.693(3) Å. Notably, only two meta-*N* atoms of *c*-N_5^- formed two hydrogen bonds: N16 formed two 2.5156(23) Å and 2.5790(291) Å hydrogen bonds with two melamine molecules; N19 formed two 2.6817(308) Å and 2.693(3) Å hydrogen bonds with two $TATOT^+$ cations (Supplementary Fig. 8). The four hydrogen bonds connecting these two nitrogen atoms were weaker than the single hydrogen bonds connecting each of the other nitrogen atoms, so the force on the *c*-N_5^- ring in all directions was relatively uniform, which increased the stability of *c*-N_5^-. In addition to the hydrogen bonding interactions on each layer, there should also be π–π interactions between adjacent *c*-N_5^- rings in adjacent layers (interlayer distance: ~3.2 Å), which further study confirmed. Along the *c*-axis, the centers of the *c*-N_5^- ions arranged in parallel in 1D pores were located on the central axes of the pores, and hydrogen bonding between the framework and *c*-N_5^- in the pores was quite dense (Fig. 3d).

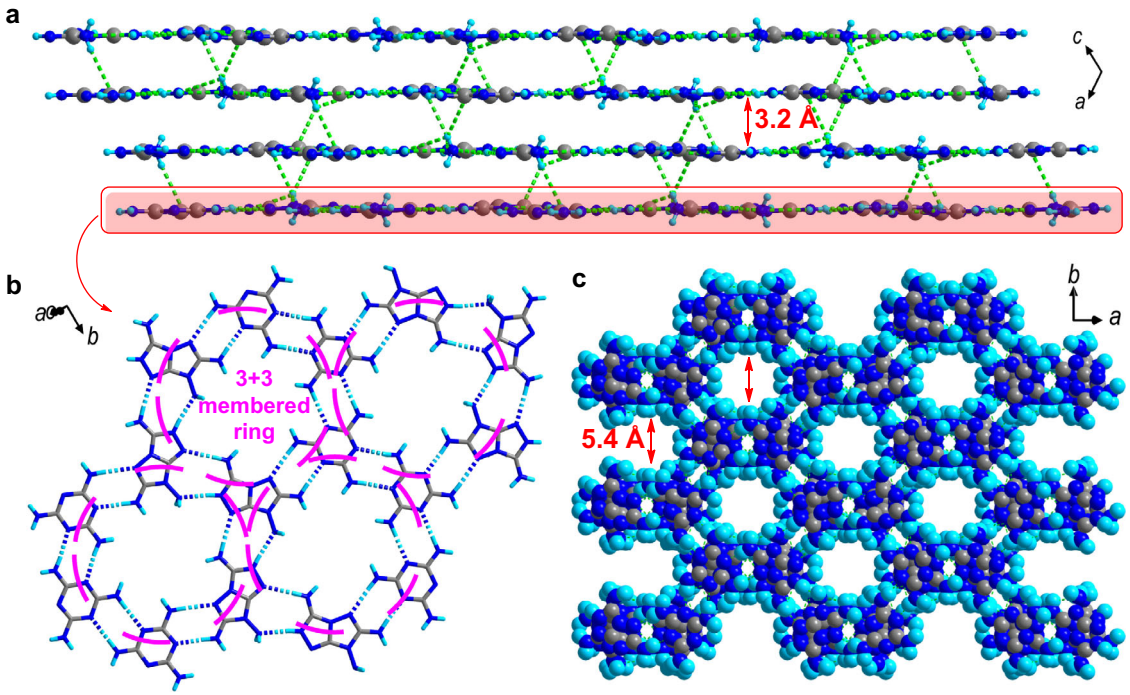

Fig. 2 | Structure of the HOF. a Layer-by-layer packing of the HOF. **b** Arrangement of 3 + 3 membered rings in a single layer. **c** HOF packing diagram with 1D pore diameters of 5.4 Å.

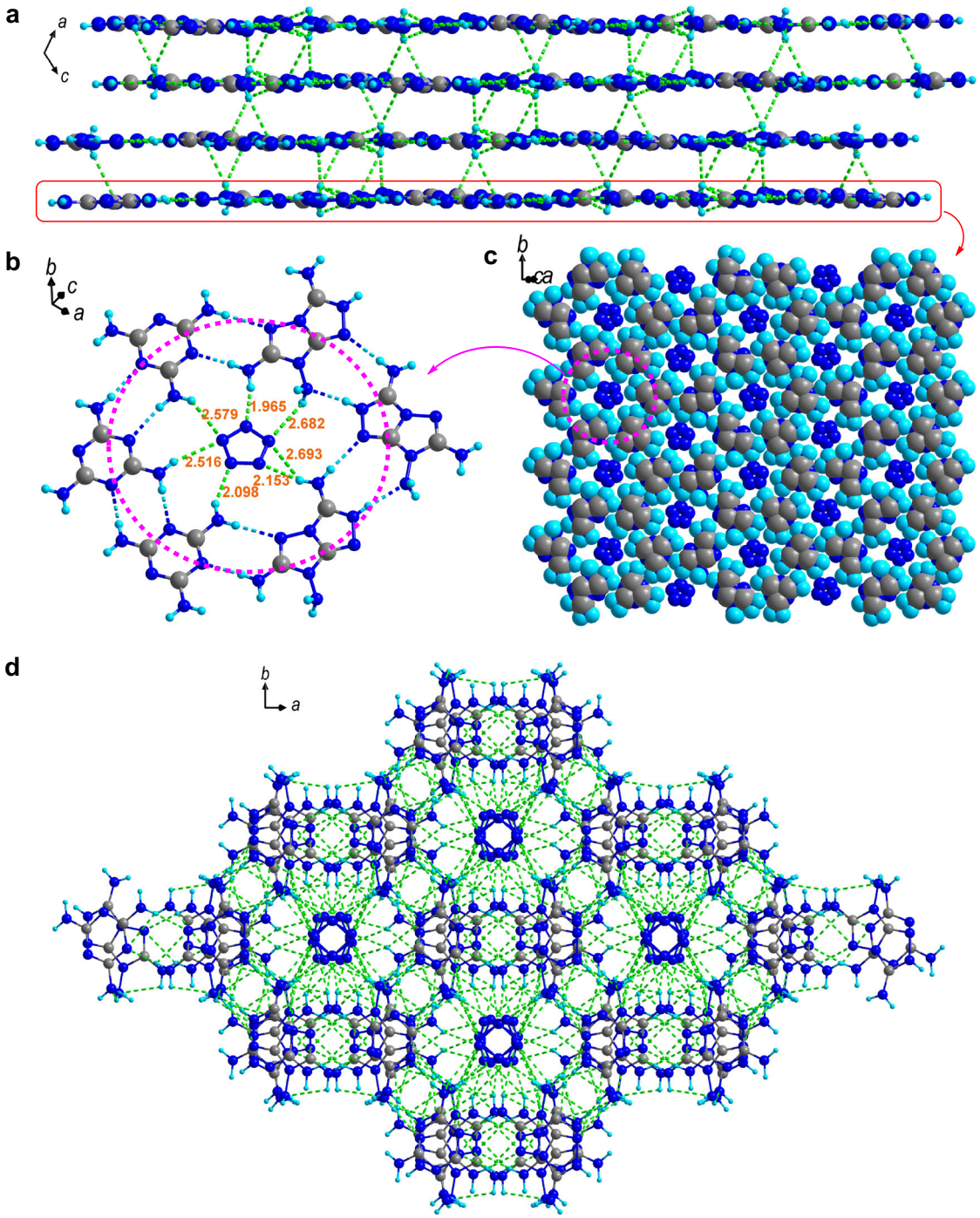

Fig. 3 | Structure of *c*-N_5^-@HOF. a Layer-by-layer packing of the *c*-N_5^-@HOF. **b** The position of *c*-N_5^- in the 3 + 3 membered ring and the hydrogen bonds (green dotted lines) accepted. **c** Arrangement of *c*-N_5^- anions in a single layer. **d** Packing diagram for *c*-N_5^-@HOF.

Thermal Stability

The thermal stability of *c*-N_5^-@HOF was determined with TG-DSC under a N_2 atmosphere with a scan rate of 5 °C min^{-1}. As shown in (Fig. 4a, *c*-N_5^-@HOF exhibited a weak exothermic peak at 161 °C followed by an obvious endothermic peak (172 °C), which corresponded to the weight loss stage starting at 133 °C on the TG curve. Based on the mass spectra (Supplementary Fig. 28) of the gaseous products (mainly N_2 ($m/z = 28$)), we concluded that *c*-N_5^- decomposed during this process. This is the first example in which the onset decomposition temperature of a *c*-N_5^- compound[13–25] exceeded 135 °C (Fig. 4c and Supplementary Table 11); it reached an unexpected value of 153 °C, indicating that the HOF significantly increased the thermal stability of *c*-N_5^-. The intense exothermic peak at 249 °C, which corresponded to a weight loss starting at 225 °C, was attributed to decomposition of the $TATOT^+$ cation[35]. This decomposition process produced peaks at $m/z = 28$, 32, 16, and 27, which indicated the production of N_2 (g), NH_2-NH_2 (g), CH_4 (g), and CHN (g), respectively. Melamine had the best thermal stability, and its endothermic sublimation peak was observed at 350 °C, which was consistent with the data (345–352 °C) reported in the literature[36,37].

The mechanical sensitivities of the *c*-N_5^-@HOF were measured with the standard BAM method. It proved to be insensitive to impact and friction (IS > 40 J and FS > 360 N), highlighting the potential for application of energetic HOFs in chemical coatings desensitization of sensitive HEDMs. The insensitivity and good thermal stability of *c*-N_5^- were the joint results of

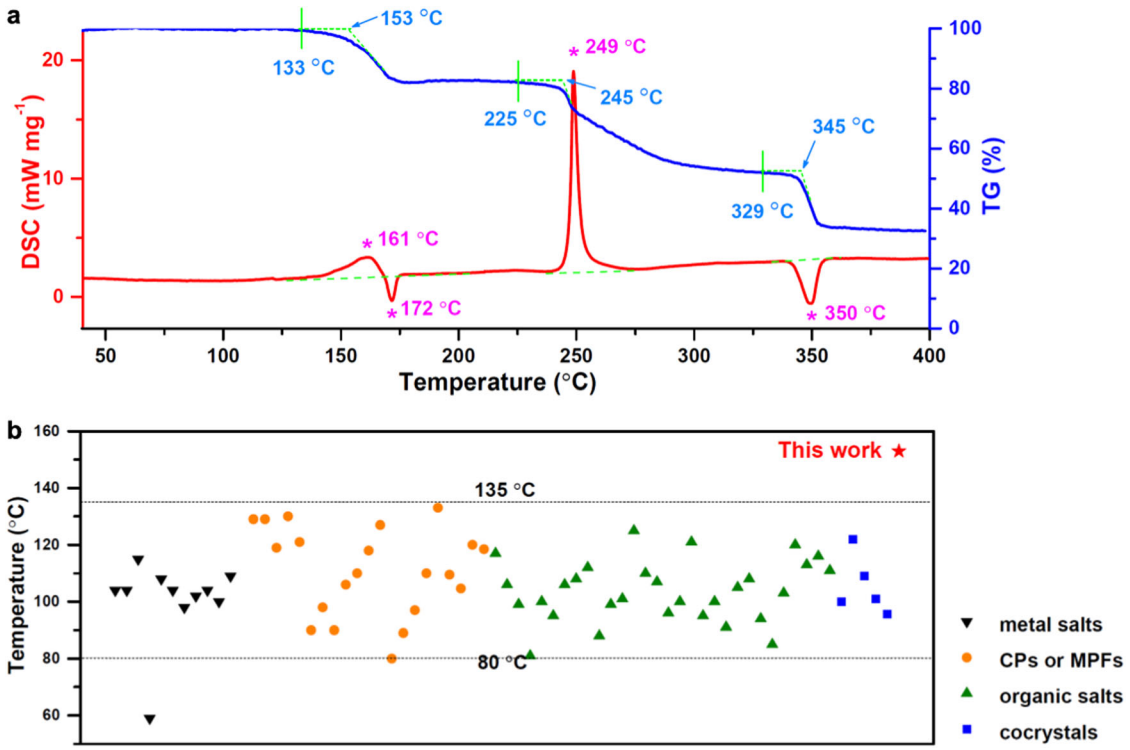

Fig. 4 | Thermal stability of *c*-N_5^-@HOF. a TG-DSC curves for *c*-N_5^-@HOF generated at a heating rate of 5 °C min^{-1} under a dry nitrogen atmosphere over the temperature range 40–400 °C. **b** Decomposition temperatures of most reported *c*-N_5^- based metal salts, CPs (coordination polymers), MPFs (metal-pentazolate frameworks), organic salts, and cocrystals.

Fig. 5 | Noncovalent interaction (NCI) plots of *c*-N_5^-@HOF. The surfaces are colored on a blue-green-red scale indicating strong attractive interactions, weak attractive, and strong non-bonded overlap, respectively (upper, layer-layer viewpoint, down, layer-layer overlap viewpoint).

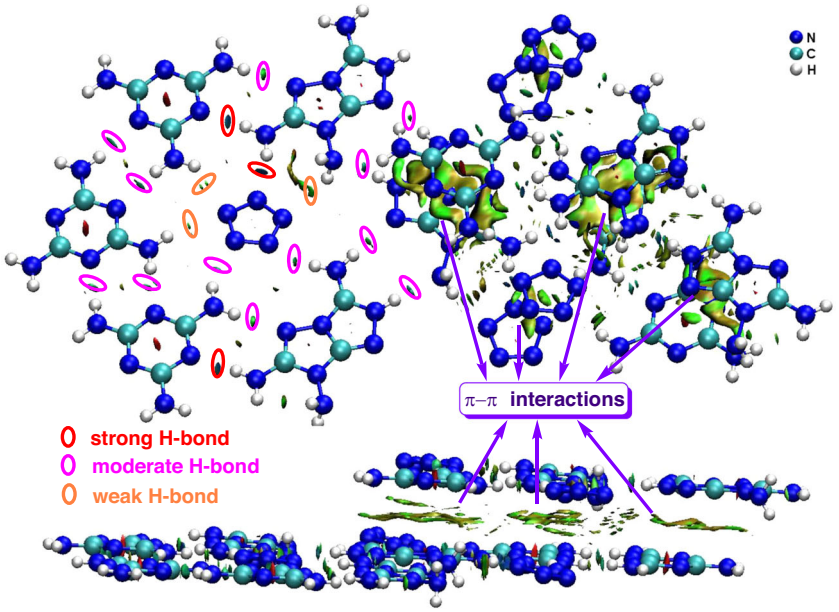

electrostatic attractions between the positive hydrogen-bonded organic framework and the negative *c*-N_5^- rings, hydrogen bonding stabilization of *c*-N_5^- by N—Hs exposed on the inner wall of each channel, and π–π interactions between adjacent *c*-N_5^- rings. A strengthened framework constructed from many paired moderate to strong hydrogen bonds is required for high stability, which was confirmed by NCI calculations[38] with Multiwfn[39] (Fig. 5 and Supplementary Fig. 10). All of the nitrogen atoms of *c*-N_5^- were surrounded by weak to moderate hydrogen bonds. In addition, there were substantially offset face-to-face π–π interactions between the *c*-N_5^- rings and the ligands (melamine molecules and fused $TATOT^+$ cations) of HOF in adjacent layers. These weak attractions created a tightly layered π–π stacked *c*-N_5^-@HOF, which resisted the influence of external heat and other factors, thus enabling the monomers to remain stably bound.

The interactions discussed above were also confirmed with a Hirshfeld surface[40] analysis within the suite of tools in CrystalExplorer17[41]. The H…N and N…H interactions designated hydrogen bonds, while C…N, N…C, C…C, and N…N interactions designated π–π interactions (Fig. 6 and Supplementary Fig. 17). The hydrogen bonding interactions appeared as red

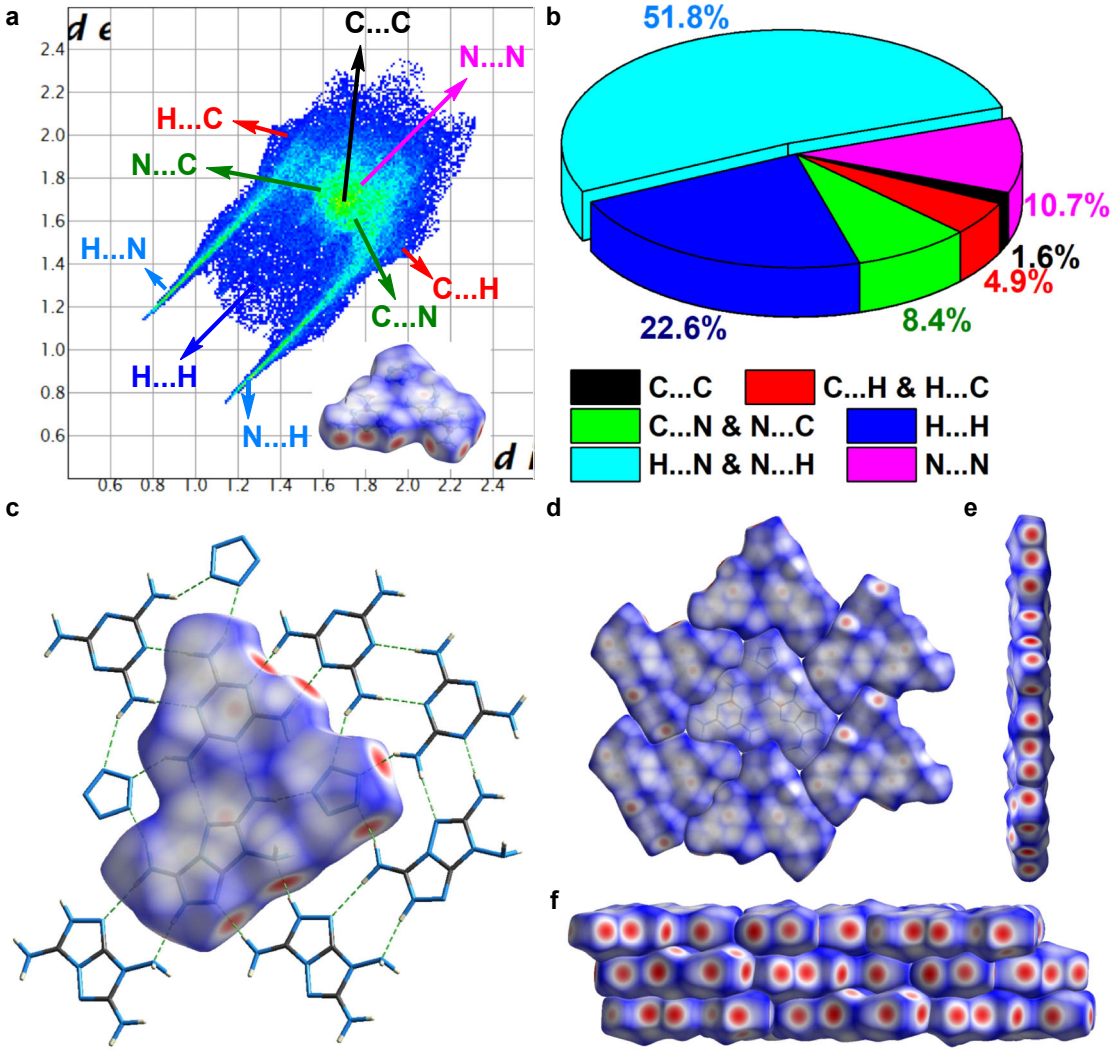

Fig. 6 | Hirshfeld surface analysis of *c*-N_5^-@HOF. a 2D fingerprint plot associated with the Hirshfeld surface. **b** Pie charts for the individual atomic contact percentages contributing to the Hirshfeld surface in *c*-N_5^-@HOF. **c**–**f** Hirshfeld surfaces for the asymmetric unit, 2D layer, and layer by layer packing.

dots on the plate Hirshfeld surface edges and were mainly distributed within the layers (Fig. 6c, e), and a few weak hydrogen bonds were distributed on the surface of the layer (Fig. 6d). These interactions (51.8 % of the total weak interactions) strengthened the 3D structure of the framework along with the π–π interactions (20.7 %) (Fig. 6f). In addition, there were also some weak H…H interactions (22.6 %) between layers, which were blue areas on the Hirshfeld surface few close contacts. As shown in Fig. 6a, a pair of remarkable spikes with $di + de$ slightly less than 2 on the bottom left in the 2D fingerprint plot indicated the presence of strong N…H hydrogen bonds, as with reported *c*-N_5^- compounds[19]. Consistent with the findings of previous studies on CHON energetic molecules[42], these hydrogen bonds and π–π interactions were also important characteristics that were insensitive to *c*-N_5^-@HOF.

Organic salts and cocrystals of *c*-N_5^- with thermal decomposition temperatures ≥ 120 °C, including biguanidinium pentazolate (T_d = 125 °C)[19], $TATOT^+N_5^- \cdot TATOT$ cocrystal (T_d = 122 °C)[43], $TATOT^+N_5^-$ (T_d = 121 °C)[19], 3,5-diamino-4-nitro-1*H*-pyrazol-2-ium pentazolate (T_d = 120 °C)[44], and 4-nitro-(3,4-diamino-1,2,4-triazolium-5-yl)-1*H*-pyrazolium pentazolate (T_d = 120 °C)[45], were selected for comparison. The ESPs[46] were calculated at the MP2/6-311++G(d,p) level and compared with that of *c*-N_5^-@HOF (Supplementary Figs. 11–16). A surface local maximum was observed above the center of the *c*-N_5^- ring for each compound. The maximum value of the ESP in *c*-N_5^-@HOF (−34.37 kcal mol^{-1}) was lower than those of the other five representative compounds (−33.68 to −24.43 kcal mol^{-1}). A lower ESP implies greater stability[47], so a strengthened framework and various weak interactions indicated a stabilized *c*-N_5^-. In terms of the Hirshfeld surfaces of the *c*-N_5^- ring in *c*-N_5^-@HOF and the other five compounds used for comparison, the N…H interactions (hydrogen bonds) of *c*-N_5^- in *c*-N_5^-@HOF accounted for the largest proportion (83.4% *vs* 55.2–82.4%) and greatest intensity (Supplementary Figs. 18–23). In addition, compared with those of biguanidinium pentazolate, the hydrogen bonds of *c*-N_5^- in *c*-N_5^-@HOF were more symmetrical, and the face-to-face π–π domains were larger and more abundant (Supplementary Fig. 10). These results also indirectly indicated that symmetrical *c*-N_5^- hydrogen bonding[48] was the main factor for stabilization of *c*-N_5^-, while face-to-face π–π stacking interactions played auxiliary roles in promoting stability.

Previous studies have shown that more symmetrical and homogeneous *c*-N_5^- hydrogen bonds are less likely to distort the *c*-N_5^- ring and lead to greater stability[48]. The undistorted *c*-N_5^- is a perfect regular pentagon, and theoretically, the most stable structure has five N—N bonds of 1.3175 Å (calculated at the M062X/6-31+G(d,p) level by Gaussian 09[49]). On this basis, the standard deviation for the N—N bond lengths in *c*-N_5^-@HOF was calculated as 6.522×10^{-3} (Supplementary Table 15). This means that from the perspective of bond length, the distortion of *c*-N_5^- in *c*-N_5^-@HOF was weaker than those in the $TATOT^+N_5^- \cdot TATOT$ cocrystal (22.616×10^{-3}), $TATOT^+N_5^-$ (9.183×10^{-3}), 3,5-diamino-4-nitro-1*H*-pyrazol-2-ium pentazolate (18.049×10^{-3}), and 4-nitro-(3,4-diamino-1,2,4-triazolium-5-yl)-

1*H*-pyrazolium pentazolate (8.434×10^{-3}). Then, to analyze the effects of distortion on the stability of *c*-N_5^-, in Supplementary Table 16, the Laplacian bond order (LBO) of the *c*-N_5^- in *c*-N_5^-@HOF was calculated with Gaussian 09[49] at the B3LYP/6-31+G(d,p) level and Multiwfn[39] to determine the covalent bond strength. A comparison of the five pentazolate compounds with thermal decomposition temperatures ≥120 °C revealed that in the *c*-N_5^-@HOF treatment, the minimum LBO value was 1.0621, which was greater than that of biguanidinium pentazolate (1.0571), $TATOT^+N_5^- \cdot TATOT$ cocrystal (0.9998), and 3,5-diamino-4-nitro-1*H*-pyrazol-2-ium pentazolate (0.9027). As is well known, a larger LBO means a higher bond dissociation energy[50] and a more stable *c*-N_5^-, which is consistent with the trend for experimental thermal stabilities. In addition, the most widely used nuclear independent chemical shift (NICS)[51] method for diagnosing aromaticity was used to analyze the aromaticities of *c*-N_5^- in *c*-N_5^-@HOF and five other compounds. As shown in Supplementary Table 17, *c*-N5$^-$@HOF exhibited the greatest aromaticity ($NICS_{ZZ}(1)$: −45.33; $NICS_{ZZ}(-1)$: −45.34). According to the analyses of bond lengths and LBO, the *c*-N_5^- rings in *c*-N_5^-@HOF were slightly distorted. Aromaticity is an important factor in maintaining the stability of *c*-N_5^-, so the *c*-N_5^- rings in *c*-N_5^-@HOF required greater aromaticity to maintain stability.

Energetic performance

As lightweight functional materials, HOFs are essentially low-density porous media without metals, and their densities are generally less than 1 g cm^{-3} [31]. However, in this study, *c*-N_5^-@HOF was constructed with energetic nitrogen-rich organic ligands instead of the commonly used arenes, and the density was 1.640 g cm^{-3} at 298 K. This density was greater than those of $TATOT^+N_5^-$ (1.615 g cm^{-3}), $TATOT^+N_5^- \cdot TATOT$ cocrystal (1.638 g cm^{-3}), and most nonmetallic *c*-N_5^- compounds[13–25]. The heat of formation for *c*-N_5^-@HOF was estimated as 787.7 kJ mol^{-1} according to the literature[52]. Using the measured density at room temperature (1.640 g cm^{-3}) and the calculated heat of formation, the detonation velocity (*D*) and pressure (*P*) of *c*-N_5^-@HOF (Supplementary Note 9 and Tables 12–13) were calculated with EXPLO5 V6.05.04 software[53]. The *D* and *P* values (8.029 km s^{-1}, 24.6 GPa) were greater than those of $TATOT^+N_5^-$ (7.791 km s^{-1}, 24.6 GPa)[19] and 2,4,6-trinitrotoluene (6.881 km s^{-1}, 19.5 GPa)[54]. Although the detonation energy of *c*-N_5^-@HOF was lower than those of explosives such as 1,3,5-trinitro-1,3,5-triazacyclohexane and 1,3,5,7-tetranitro-1,3,5,7-tetraazacycloocatane, its thermal stability was one step closer to the application standard, and it is also a candidate insensitive material.

Discussion

A nitrogen-rich HOF with 1D pores was designed and obtained by self-assembly, and *c*-N_5^- anions occupied the pores and were stabilized by many hydrogen bonds with the HOF, π–π interactions between the five-membered rings, and attraction of the anions with the cationic HOF. These factors resulted in *c*-N_5^-@HOF thermal stability up to 153 °C, surpassing those of all reported *c*-N_5^- based compounds. We believe that this strategy will open the door to stable *c*-N_5^- and overcome the problem of poor *c*-N_5^- thermal stability by encapsulating it in HOFs. It is likely that HOFs with increasingly high energies, composed of energetic N—H- and/or O—H-rich ligands, will be used to capture and stabilize *c*-N_5^- while exhibiting excellent thermal stabilities and improved detonation properties.

Materials and methods

Safety precautions

Although no explosions or hazards were observed during the preparation and handling of these compounds in this work, all of the compounds investigated are potentially energetic materials. Scratching or scraping of these energetic materials must be avoided. Laboratories and personnel must be properly grounded, and safety equipment such as protective gloves and coats, face shields, and explosion-proof baffles are recommended. In addition, all of the compounds must be synthesized only on small scales.

General methods

All reagents and solvents were purchased from Sigma-Aldrich, Aladdin, and Energy Chemical (analytical grade) and were used as received.

^{1}H NMR and ^{13}C NMR spectra were recorded using a 500 MHz (Bruker AVANCE III 500) nuclear magnetic resonance spectrometer operating at 500 and 125.72 MHz, respectively. Chemical shifts in the ^{1}H NMR and ^{13}C NMR spectra are reported relative to Me_4Si as external standard. Single-crystal X-ray diffraction was conducted with a Bruker D8 QUEST PHOTON 100 diffractometer using Mo-Kα radiation (λ = 0.71073 Å) (please refer to Supplementary Note 1 for detailed information). High-resolution mass spectra (electrospray ionization) were recorded with a Thermo Fisher Q Exactive Focus high-resolution mass spectrometer operated in splitless mode. The samples were dissolved in methanol (10 ppm), and introduced via a syringe pump at 30 μL min^{-1}. The instrument was run with an electrospray voltage of 3.0 kV. DSC plots were acquired with a differential scanning calorimeter (NETZSCH DSC 204 F1 Phoenix) at a scan rate of 5 °C min^{-1} in perforated Al containers under a nitrogen flow of 60 mL min^{-1}. TG-DSC measurements were performed with a NETZSCH STA 449 F5 Jupiter system at a heating rate of 5 °C min^{-1} under a nitrogen atmosphere. TG/DTA-MS was performed with a Rigaku Thermo Plus EV2/Thermo mass Photothermal Analyzer at a heating rate of 5 °C min^{-1} under a nitrogen atmosphere. IR spectra were recorded with a Thermo Nicolet iS10 spectrometer equipped with a Thermo Scientific Smart iTR diamond ATR accessory. Elemental analyses were carried out with a Vario EL III CHNOS elemental analyzer. Densities were measured at 25 °C with an Anton Paar Ultrapyc 5000 gas pycnometer. Impact and friction sensitivity measurements were performed with a standard BAM Fall hammer and a BAM friction tester.

Synthetic procedures

AgN_5, melamine hydrochloride, and TATOT are synthesized according to the literature[19,34,35].

MaN_5. A solution of melamine hydrochloride (730 mg, 4.5 mmol) in distilled water (10 mL) was added dropwise to a suspension of AgN_5 (800 mg, 4.5 mmol) in distilled water (15 mL). The mixture was reacted in the dark for 0.5 h, after which the mixture was centrifuged and filtered. The obtained filtrate was concentrated under reduced pressure to give the desired MaN_5 (797 mg, yield: 90 %). The solid products were recrystallized in methanol/water to obtain white crystals. $T_{d,\ onset}$: 110 °C (DSC). ^{1}H NMR: δ 7.72 ppm; ^{13}C NMR: δ 159.79 ppm. HRMS (*m/z*): $[M]^+$: 127.07 (Ma^+); $[M]^-$: 70.01 (*c*-N_5^-). IR (ATR): $\tilde{\nu}$ 3337, 3155, 1681, 1702, 1632, 1537, 1456, 1394, 1218, 1171, 1010, 880, 813, 781, 750, 718 cm^{-1}. Elemental analysis for $C_3H_7N_{11}$ (197.166): calcd C 18.28, H 3.58, N 78.15 %. Found: C 18.22, H 3.55, N 78.21 %. IS: >40J; FS: >360N.

***c*-N_5^-@HOF.** MaN_5 (197 mg, 1 mmol) and TATOT (254 mg, 1 mmol) were dissolved in 10 mL of distilled water, and the reaction mixture was slowly heated to 40 °C and stirred for 2 h. After the reaction, the mixture was cooled to room temperature and filtered, and the filtrate was slowly evaporated at room temperature for 3–4 days to obtain slightly yellow crystals. Yield: 70 %. $T_{d,\ onset}$: 153 °C (TG). ^{1}H NMR: δ 9.62, 8.23, 8.03, 7.28, 5.88 ppm; ^{13}C NMR: δ 164.06, 159.96, 148.23, 142.42 ppm. HRMS (*m/z*): $[M]^+$: 127.073 (Ma^+), 155.050 (TATOT + H^+) $[M]^-$: 70.015 (*c*-N_5^-). IR (ATR): $\tilde{\nu}$ 3411, 3301, 3115, 2028, 1687, 1635, 1537, 1455, 1414, 1263, 1216, 1159, 1099, 1021, 939, 842, 811, 723, 702 cm^{-1}. Elemental analysis for $C_6H_{13}N_{19}$ (351.303): calcd C 20.51, H 3.73, N 75.76 %. Found: C 20.55, H 3.80, N 75.69 %. IS: >40J; FS: >360N.

Data availability

The data that support the findings of this study are available from the corresponding author upon reasonable request. The X-ray crystallographic coordinates for structures reported in this Article have been deposited at the Cambridge Crystallographic Data Centre (CCDC), under deposition number CCDC 2286232 and 2286237. These data can be obtained free of

charge from The Cambridge Crystallographic Data Centre via www.ccdc.cam.ac.uk/data_request/cif.

Received: 7 September 2023; Accepted: 27 February 2024;
Published online: 07 March 2024

References

1. Klapötke T. M. *Chemistry of High-energy materials* 4th edition, (Walter de Gruyter GmbH, Berlin/Boston, 2017).
2. Christe, K. O. Recent advances in the chemistry of N_5^+, N_5^- and high-oxygen compounds. *Propell. Explos. Pyrotech.* **32**, 194–204 (2007).
3. Gozin M., Fershtat L. L. *Nitrogen-rich energetic materials*, (WILEY-VCH GmbH, Weinheim, Germany, 2023).
4. Singh, R. P., Verma, R. D., Meshri, D. T. & Shreeve, J. M. Energetic nitrogen-rich salts and ionic liquids. *Angew. Chem., Int. Ed.* **45**, 3584–3601 (2006).
5. Zarko, V. E. Searching for ways to create energetic materials based on polynitrogen compounds (review). *Combust. Explos. Shock Waves* **46**, 121–131 (2010).
6. O'Sullivan, O. T. & Zdilla, M. J. Properties and promise of catenated nitrogen systems as high-energy-density materials. *Chem. Rev.* **120**, 5682–5744 (2020).
7. Wozniak, D. R. & Piercey, D. G. Review of the current synthesis and properties of energetic pentazolate and derivatives thereof. *Engineering* **6**, 981–991 (2020).
8. Curtius, T. "The azide ion,". *Berichte Dtsch. Chem. Ges.* **23**, 3023 (1890).
9. Christe, K. O., Wilson, W. W., Sheehy, J. A. & Boatz, J. A. N_5^+: a novel homoleptic polynitrogen ion as a high energy density material. *Angew. Chem. Int. Ed.* **38**, 2004–2009 (1999).
10. Zhang, C., Sun, C., Hu, B., Yu, C. & Lu, M. Synthesis and characterization of the pentazolate anion *cyclo*-N_5^- in $(N_5)_6(H_3O)_3(NH_4)_4Cl$. *Science* **355**, 374–376 (2017).
11. Christe, K. O. Polynitrogen chemistry enters the ring. *Science* **355**, 351 (2017).
12. Xu, Y. et al. A series of energetic metal pentazolate hydrates. *Nature* **549**, 78–81 (2017).
13. Wang, P., Xu, Y., Lin, Q. & Lu, M. Recent advances in the syntheses and properties of polynitrogen pentazolate anion *cyclo*-N_5^- and its derivatives. *Chem. Soc. Rev.* **47**, 7522–7538 (2018).
14. Zhang, C. et al. A symmetric $Co(N_5)_2(H_2O)_4{\cdot}4H_2O$ high-nitrogen compound formed by cobalt(II) cation trapping of a cyclo-N_5^- anion. *Angew. Chem., Int. Ed.* **56**, 4512–4514 (2017).
15. Zhang, W. et al. Stabilization of the pentazolate anion in a zeolitic architecture with $Na_{20}N_{60}$ and $Na_{24}N_{60}$ nanocages. *Angew. Chem., Int. Ed.* **57**, 2592–2595 (2018).
16. Sun, C. et al. Synthesis of AgN_5 and its extended 3D energetic framework. *Nat. Commun.* **9**, 1269 (2018).
17. Xu, Y., Lin, Q., Wang, P. & Lu, M. Stabilization of the pentazolate anion in three anhydrous and metal-free energetic salts. *Chem. Asian J.* **13**, 924–928 (2018).
18. Yang, C. et al. Synthesis and characterization of *cyclo*-pentazolate salts of NH_4^+, NH_3OH^+, $N_2H_5^+$, $C(NH_2)_3^+$, and $N(CH_3)_4^+$. *J. Am. Chem. Soc.* **140**, 16488–16494 (2018).
19. Xu, Y., Tian, L., Li, D., Wang, P. & Lu, M. A series of energetic *cyclo*-pentazolate salts: rapid synthesis, characterization, and promising performance. *J. Mater. Chem. A* **7**, 12468–12479 (2019).
20. Luo, J., Xia, H., Zhang, W., Song, S. & Zhang, Q. A promising hydrogen peroxide adduct of ammonium cyclopentazolate as a green propellant component. *J. Mater. Chem. A* **8**, 12334–12338 (2020).
21. Xu, Y. et al. LiN_5: a novel pentazolate salt with high nitrogen content. *Chem. Eng. J.* **429**, 132399 (2022).
22. Zhou, J. et al. Improving the stability of hydrazinium pentazolate through cocrystallization. *CrystEngComm* **25**, 2027–2031 (2023).
23. Yuan, Y. et al. Pentazolate coordination polymers self-assembled by in situ generated $[Pb_4(OH)_4]^{4+}$ cubic cations trapping *cyclo*-N_5^-. *Dalton Trans* **51**, 5801–5809 (2022).
24. Xu, Y. et al. Hexaamminecobalt(III) cation as multiple hydrogen bond donors: synthesis, characterization and energetic properties of *cyclo*-pentazolate and azide based complexes. *Cryst. Growth Des.* **23**, 811–819 (2023).
25. Cao, Y., Xia, H., Wang, K., Zhang, Q. & Zhang, W. Structural analysis and controllable fabrication of two pentazolate-based 3D topological networks. *Inorg. Chem.* **60**, 8409–8413 (2021).
26. Xu, Y. et al. A low sensitivity energetic cocrystal of ammonium pentazolate. *J. Energ. Mater.* **41**, 99–116 (2023).
27. Vij, A. et al. Polynitrogen chemistry. Synthesis, characterization, and crystal structure of surprisingly stable fluoroantimonate salts of N_5^+. *J. Am. Chem. Soc.* **123**, 6308–6313 (2001).
28. Wilson, W. W., Vij, A., Vij, V., Bernhardt, E. & Christe, K. O. Polynitrogen chemistry: preparation and characterization of $(N_5)_2SnF_6$, N_5SnF_5, and $N_5B(CF_3)_4$. *Chem. Eur. J.* **9**, 2840–2844 (2003).
29. Haiges, R., Schneider, S., Schroer, T. & Christe, K. O. High-energy-density materials: synthesis and characterization of $N_5^+[P(N_3)_6]^-$, $N_5^+[B(N_3)_4]^-$, $N_5^+[HF_2]^-{\cdot}n$HF, $N_5^+[BF_4]^-$, $N_5^+[PF_6]^-$, and $N_5^+[SO_3F]^-$. *Angew. Chem., Int. Ed.* **43**, 4919–4924 (2004).
30. Yang, Y. et al. Ethylene/ethane separation in a stable hydrogen-bonded organic framework through a gating mechanism. *Nat. Chem.* **13**, 933–939 (2021).
31. Lin, R. B. et al. Multifunctional porous hydrogen-bonded organic framework materials. *Chem. Soc. Rev.* **48**, 1362–1389 (2019).
32. Song, X. et al. Design rules of hydrogen-bonded organic frameworks with high chemical and thermal stabilities. *J. Am. Chem. Soc.* **144**, 10663–10687 (2022).
33. Zhang, J., Feng, Y., Staples, R. J., Zhang, J. & Shreeve, J. M. Taming nitroformate through encapsulation with nitrogen-rich hydrogen-bonded organic frameworks. *Nat. Commun.* **12**, 2146 (2021).
34. Dou, M., Wang, J., Gao, B., Xu, C. & Yang, F. Photocatalytic difference of amoxicillin and cefotaxime under visible light by mesoporous g-C_3N_4: Mechanism, degradation pathway and DFT calculation. *Chem. Eng. J.* **383**, 123134 (2020).
35. Klapötke, T. M., Schmid, P. C., Schnell, S. & Stierstorfer, J. 3,6,7-Triamino-[1,2,4]triazolo[4,3-*b*][1,2,4]triazole: A non-toxic, high-performance energetic building block with excellent stability. *Chem. Eur. J.* **21**, 9219–9228 (2015).
36. Kurzer F. & Powell J. R. Cyanamides. Part VI. Sulphonyl derivatives related to dicyandiamide and melamine. *J. Chem. Soc*. 2531–2537 https://pubs.rsc.org/en/content/articlelanding/1953/jr/jr9530002531 (1953).
37. Bradley, E. L., Castle, L., Jickells, S. M., Mountfort, K. A. & Read, W. A. Use of overall migration methodology to test for food-contact substances with specific migration limits. *Food Addit. Contam. A* **26**, 574–582 (2009).
38. Johnson, E. R. et al. Revealing noncovalent interactions.*J. Am. Chem. Soc.* **132**, 6498–6506 (2010).
39. Lu, T. & Chen, F. Multiwfn: a multifunctional wavefunction analyzer. *J. Comput. Chem.* **33**, 580–592 (2012).
40. Spackman, M. A. & Jayatilaka, D. Hirshfeld surface analysis. *CrystEngComm* **11**, 19–32 (2009).
41. Turner M. J. et al. CrystalExplorer17, University of Western Australia, 2017. http://hirshfeldsurface.net.
42. Bu, R., Xiong, Y., Wei, X., Li, H. & Zhang, C. Hydrogen bonding in CHON-containing energetic crystals: a review. *Cryst. Growth Des.* **19**, 5981–5997 (2019).
43. Yang, C. et al. Investigating the stabilizing forces of pentazolate salts. *ACS Appl. Energy Mater.* **4**, 146–153 (2021).
44. Yu, R., Liu, Y., Zeng, Z., Huang, W. & Tang, Y. Synthesis and properties of a novel energetic salt 3,5-diamino-4-nitro-1*H*-pyrazol-2-ium pentazolate. *Chin. J. Energ. Mater.* **30**, 222–227 (2022).

45. Yang, C. et al. Anion-cation bonding and structure-property relationships of three *cyclo*-pentazolate compounds. *Cryst. Growth Des.* **21**, 4329–4336 (2021).
46. Zhang, J. & Lu, T. Efficient evaluation of electrostatic potential with computerized optimized code. *Phys. Chem. Chem. Phys.* **23**, 20323–20328 (2021).
47. Wang, Y. et al. A comparative study of the structure, energetic performance and stability of nitro-NNO-azoxy substituted explosives. *J. Mater. Chem. A* **2**, 20806–20813 (2014).
48. Li, X. et al. Symmetrical *cyclo*-N_5^- hydrogen bonds: stabilization mechanism of four non-metallic *cyclo*-pentazolate energetic salts. *Phys. Chem. Chem. Phys.* **24**, 3970–3983 (2022).
49. Frisch M. J. et al. Gaussian 09, Revision A.02, Gaussian, Inc., Wallingford, CT, (2009).
50. Lu, T. & Chen, F. Bond order analysis based on the laplacian of electron density in fuzzy overlap space. *J. Phys. Chem. A* **117**, 3100–3108 (2013).
51. Chen, Z. et al. Nucleus-independent chemical shifts (NICS) as an aromaticity criterion. *Chem. Rev.* **105**, 3842–3888 (2005).
52. Foroughi, L. M., Wiscons, R. A., Bois, D. R. D. & Matzger, A. J. Improving stability of the metal-free primary energetic cyanuric triazide (CTA) through cocrystallization. *Chem. Commun.* **56**, 2111–2114 (2020).
53. Sućeska M. EXPLO5 V6.05.04 Brodarski Institute (2020).
54. Xu, Y. et al. Syntheses, structures, and properties of polynitro-substituted 5,6-dihydrodiimidazo[1,2-*a*:2',1'-*c*]pyrazine energetic compounds. *Cryst. Growth Des.* **22**, 3914–3923 (2022).

Acknowledgements

This work was supported by the National Natural Science Foundation of China (no. 22105102, 22135003, and 21975127), Young Elite Scientist Sponsorship Program by CAST (no. YESS20210074), and the Fundamental Research Funds for the Central Universities (no. 30921011204). We thank Mr. S. Jiang (Nanjing University of Science and Technology) for the aromaticity calculation.

Author contributions

Y.X. and M.L. designed the study. J.Z., X.L., T.H., Z.X., and P.W. performed the reactions and characterizations. Y.X. finished most of the theoretical calculations. Y.X. and J.Z. prepared the original manuscript, which was then reviewed by M.L. All the authors discussed the results of this article.

Competing interests

The authors declare no competing interests.

Additional information

Supplementary information The online version contains supplementary material available at https://doi.org/10.1038/s43246-024-00467-7.

Correspondence and requests for materials should be addressed to Yuangang Xu or Ming Lu.

Peer review information *Communications Materials* thanks the anonymous reviewers for their contribution to the peer review of this work. Primary Handling Editor: Jet-Sing Lee.